Inorganic Chemistry

Article

pubs.acs.org/IC

Rhodium Complexes of a Chelating Ligand with Imidazol-2-ylidene and Pyridin-2-ylidene Donors: The Effect of *C*-Metalation of Nicotinamide Groups on Uptake of Hydride Ion

Alex McSkimming, Graham E. Ball, Mohan M. Bhadbhade, and Stephen B. Colbran*

School of Chemistry, The University of New South Wales, Sydney, NSW 2052 Australia

Supporting Information

ABSTRACT: Rhodium complexes of the imidazolylidene (*C*-im) *N*-heterocyclic carbene (NHC) ligand, *C*-im-pyH$^+$, bearing a nicotinamide cation substituent (pyH$^+$) have been targeted for ligand-centered uptake and delivery of hydride ion. This work reveals that rhodium(I) complexes such as [Rh(*C*-im-pyH$^+$)(COD)X][PF$_6$] (**1**, **a**: X = Cl, **b**: X = I) undergo facile *C*-metalation of the nicotinamide ring to afford rhodium complexes of a novel chelate ligand, *C*,*C*′-im-py, with coordinated imidazolylidene (C$_{im}$) and pyridylidene (C$_{py}$) NHC-donors. Seven examples were characterized and include rhodium(III) monomers of the general formula [Rh(*C*,*C*′-im-py)L$_x$I$_2$]$^{z+}$ (**2**: z = 1, L = H$_2$O or solvent, x = 2; **3**, **5**, **7**: z = 0, L = carboxylate, x = 1) and novel rhodium(II) dimers, the *anti*/*syn*-isomers of [Rh$_2$(*C*,*C*′-im-py)$_2$(μOAc)$_2$I$_2$] (**4**-***anti***/***syn***). The NMR data, backed by DFT calculations, is consistent with attribution of the *C*,*C*′-im-py ligand as a bis(carbene) donor. Single crystal X-ray diffraction studies are reported for **2**, **3**, **4**-***anti***, **4**-***syn*** and **7**. Consistently, within the each complex, the Rh−C$_{im}$ bond length is shorter than the Rh−C$_{py}$ bond length, which is the opposite trend to that expected based on simple electronic considerations. It is proposed that intramolecular steric interactions imposed by different rings in the rigid *C*,*C*′-im-py chelate ligand dictate the observed Rh−C$_{NHC}$ bond lengths. Attempts to add hydride to the *C*-metalated nicotinamide ring in **3** were unsuccessful. The redox behavior of **3** and **4** and, for comparison, an analogous bis(imidazolylidene)rhodium(III) monomer (**8**), were characterized by cyclic voltammetry, electron paramagnetic resonance (EPR), and UV−vis spectroelectrochemistry. In **3** and **4**, the *C*-metalated nicotinamide ring is found to exhibit a one-electron reduction process at far lower potential (−2.34 V vs. Fc$^+$/Fc in acetonitrile) than the two-electron nicotinamide cation-dihydronicotinamide couple found for the corresponding nonmetalated ring (−1.24 V). The *C*,*C*′-ligand is electrochemically silent over a large potential range (from −2.3 V to the anodic solvent limit), thus for both **3** and **4** the first reduction processes are metal-centered. For **4**-***anti***, the cyclic voltammetry and UV−vis spectrochemical results are consistent with a diamagnetic [Rh(I)Rh(II)]$_2$ tetrameric reduction product. Density functional theory (DFT) calculations were used to further probe the uptake of hydride ion by the nicotinamide ring, both before and after *C*-metalation. It is found that *C*-metalation significantly decreases the ability of the nicotinamide ring to take up hydride ion, which is attributed to the "carbene-like" character of a *C*-metalated pyridylidene ring.

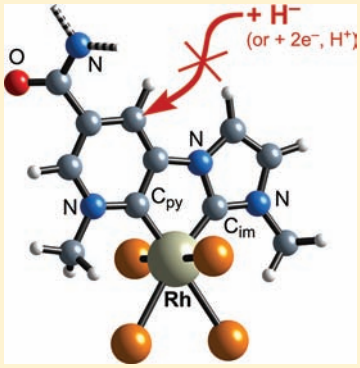

INTRODUCTION

In organic synthesis there has been a recent surge in the use of organic hydride donors such as Hantzsch esters and dihydronicotinamides as "green" and safe alternatives to inorganic reducing reagents such as sodium borohydride, lithium aluminum hydride, and molecular hydrogen.[1] In these "transfer hydrogenation" reactions, a Lewis acid, either a proton or a metal ion, usually catalyzes transfer of hydride from the organo-hydride to the substrate.[1h−m,2] The role of the Lewis acid is to bind and activate the substrate to hydride transfer; the organo-hydride is deactivated in any adducts with the Lewis acid (albeit by less than activation of the substrate), a simple consequence of polarization and charge effects.[2]

Overall, in the transfer hydrogenation reactions the organo-hydride is stoichiometrically consumed. Regeneration of the organo-hydride from its conjugate cation is thwart with difficulties: for example, radical coupling and other decomposition reactions occur upon electrochemical reduction,[3] and reduction with inorganic hydride sources is not regioselective,[4] as well as being highly inefficient. However, over the past two decades, much effort has been expended to discover, and then understand, catalysts for the regeneration of the biological organo-hydride donors, nicotinamide adenine dinucleotide (phosphate) (NAD(P)H), from their conjugate pyridinium cations, NAD(P)$^+$. The impetus was to use the NAD(P)H to drive enzyme-catalyzed organic reduction and oxidation reactions. The most prominent catalysts discovered for the regeneration of NAD(P)H are [Cp*Rh(diimine)(H$_2$O)]$^{2+}$ (diimine = derivatives of 2,2′-bipyridine and 1,10-phenanthroline).[5] These rhodium(III) complexes form hydrido-rhodium(III) (Rh^{III}−H) species upon electrochemical reduction[5g] or upon reaction with reagents such as formate,[5a−d,g−j] phosphite,[5e] or even molecular hydrogen.[5f] The Rh^{III}−H species

Received: October 5, 2011
Published: February 6, 2012

   dx.doi.org/10.1021/ic202164v | Inorg. Chem. 2012, 51, 2191−2203

regioselectively transfer hydride to NAD(P)$^+$ and simple nicotinamide cation analogues to efficiently form NAD(P)H or the corresponding dihydronicotinamide hydride donor. Studies of the catalytic regeneration of other organo-hydride donors are scarce; for example, there has been a single very recent report of catalytic regeneration of Hantzsch's ester,[6] and regeneneration of dihydrobenzimidazolidines, a class of powerful organo-hydride donors,[7] is yet to be reported.

In response to the above background, we sought to make and investigate the chemistry of transition metal complexes that incorporate (*i*) a reactive metal center capable of binding and, thereby, activating a substrate(s) and, potentially, capable of catalyzing regeneration of an organo-hydride donor, and (*ii*) an organo-hydride donor center as part of a ligand that may transfer hydride ion to the bound substrate. We reported previously the synthesis of some rhodium(I) complexes bound by an imidazolium-derived *N*-heterocyclic carbene donor (im) group with a nicotinium cation (pyH$^+$) substituent ([Rh(im-pyH$^+$)(COD)X][PF$_6$] (**1**; **a**: X = Cl, **b**: X = I; COD = 1,5 cyclooctadiene).[8] Electrolysis experiments revealed **1b**$^+$ underwent clean electrochemical reduction to afford the corresponding dihydropyridine complex, Scheme 1. This raised the prospect that complexes **1**$^+$ could be employed as electrocatalysts for reductions of organic substrates.

Scheme 1. Redox Behavior of 1$^+$

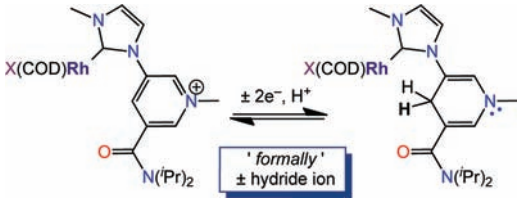

As a prelude to electrocatalysis studies, we have investigated and describe herein some simple reaction chemistry of **1**$^+$. When considering possible reactions employing **1**$^+$ as the catalyst, it was anticipated that the coordinatively labile 1,5-cyclooctadiene ligand would be substituted by the (organic) substrates. To explore the reaction chemistry of this potentially active site, we examined cyclooctadiene-substitution reactions with simple ligands such as carbon monoxide, triphenylphosphine and bis(diphenylphosphino)ethane and 2,2′-bipyridine. Analogous reactions have been employed for numerous similar complexes and usually occur rapidly and in high yield.[9] However, it was found that the pyridinium ring in **1**$^+$ is particularly susceptible to cyclometalation to afford rhodium complexes of a novel chelating ligand, *C,C*′-im-py, with imidazol-2-ylidine and pyridin-2-ylidene NHC-donor groups. A number of rhodium(III) and rhodium(II) complexes bearing the *C,C*′-im-py ligand were isolated. In the new complexes, the *C,C*′-im-py ligand is redox-inert over a wide potential range: it could not be reduced to the corresponding dihydropyridine. Density functional theory (DFT) calculations were performed to investigate reasons for this behavior.

RESULTS AND DISCUSSION

Syntheses. In a typical attempted substitution reaction, **1b** was dissolved in anhydrous, anaerobic tetrahydrofuran and treated with carbon monoxide. The solution slowly changed color from orange-red to yellow. After stirring for an hour, the solvent was removed, and ^{1}H NMR analysis of the solid residue performed. The ^{1}H NMR spectrum at this point showed numerous peaks indicative of a complex mixture of products; likewise numerous products were observed by qualitative thin-layer chromatography. Similarly, attempted substitution reactions of the 1,5-cyclooctadiene ligand in **1b** with triphenylphosphine, pyridine, 2,2′-bipyridine, 1,10-phenanthroline, and 1,2-diphenylphosphinoethane also gave complicated mixtures of many products. The low-yields of the individual products precluded their isolation.

A simple modification to our previously reported synthesis of **1b**[8] completely changed the outcome. Complex **1b** was obtained by treating [Rh(COD)Cl]$_2$ and [Him-pyH]I$_2$ in acetonitrile with triethylamine, followed by treatment with aqueous potassium hexafluorophosphate to precipitate the product. At this point, in an attempt to obtain crystalline product, acetone was added until the precipitated product redissolved. The solution was left to slowly evaporate in air, which resulted in crystallization of the rhodium(III) complex [Rh(*C,C*′-im-py)(H$_2$O)$_2$I$_2$][PF$_6$] (**2**) (70% yield, Scheme 2) in which the pyridinium ring is *C*-metalated at the *ortho*-position. The facile *C*-metalation explains the mixtures of products found in the attempted substitution reactions. Inspection of the NMR spectra following these reactions shows that many of the products also contain the *C,C*′-im-py ligand.

Crabtree and Peris reported that that reactions of [RhCl(COD)]$_2$ with imidazolium salts, excess potassium iodide, and a base afford a straightforward route to bis(imidazolylidene)-rhodium(III) complexes.[10] Following isolation of **2**, we tested whether the Crabtree–Peris route would provide a more general route to similar complexes of the novel *C,C*′-im-py chelate ligand. Thus [RhCl(COD)]$_2$, [Him-pyH]I$_2$, and excess sodium acetate and sodium iodide were heated in anhydrous, anaerobic acetonitrile. The reaction yielded the anticipated

Scheme 2. Synthesis of Complex 2

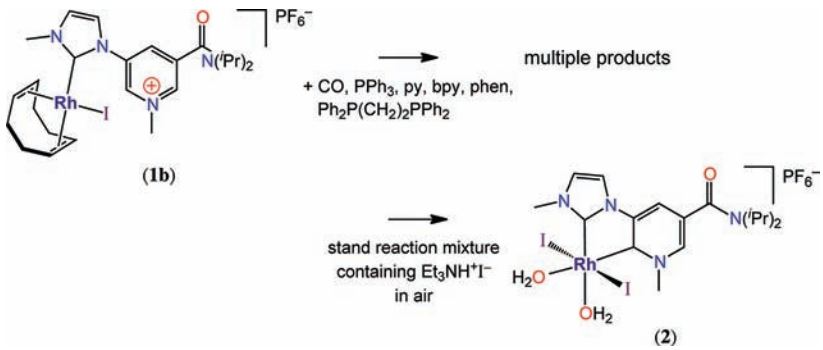

dx.doi.org/10.1021/ic202164v | *Inorg. Chem.* 2012, 51, 2191–2203

Scheme 3. Synthesis of Complexes 3−7

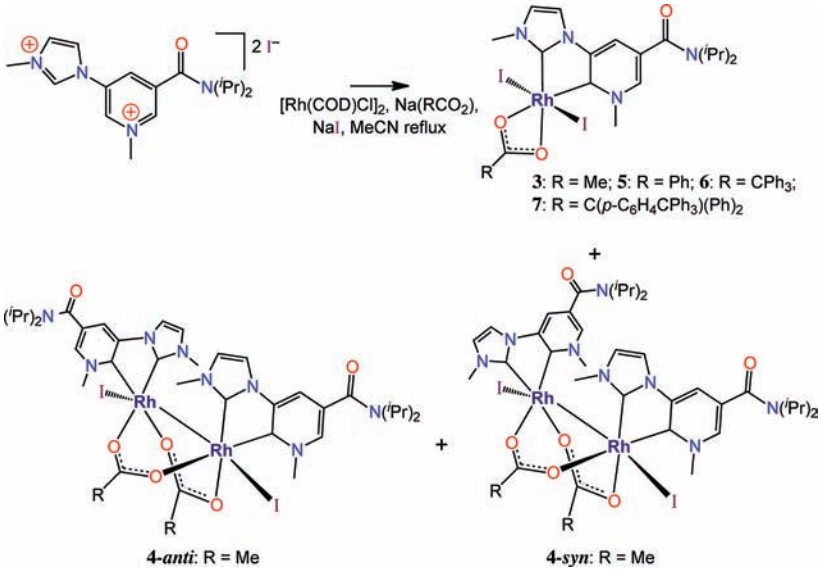

rhodium(III) complex, [Rh(*C*,*C*′-im-py)(OAc)I_2] (**3**), along with two novel rhodium(II) dimers [Rh_2(*C*,*C*′-im-py)$_2$(OAc)$_2I_2$] (**4-*anti*** and **4-*syn***), (Scheme 3). Carboxylates other than acetate were also employed in the above synthesis, and yielded analogous products. However, the *syn*/*anti*-rhodium(II) dimers with other carboxylate ligands could not be separated. For example, only [Rh(*C*,*C*′-im-py)($PhCO_2$)I_2] (**5**) was cleanly isolated from the reaction using sodium benzoate.

Inspection of the crystal structures of **4-*syn*** and **4-*anti*** (see below) suggested bulky carboxylates should repress dimer formation because of steric interactions between the bulky groups. To test this idea, [RhCl(COD)]$_2$ and potassium iodide were treated with the triphenylmethylcarboxylate anion, generated in situ by metalation of trityl chloride with sodium and passing carbon dioxide through the resulting red solution. Monitoring of the rhodium-containing mixture revealed only slow reaction. Whereas complete consumption of [RhCl(COD)]$_2$ was always observed within 5 h with the less bulky carboxylates, with $Ph_3CCO_2^-$ trace [RhCl(COD)]$_2$ remained after 5 days. At this point the reaction was stopped and the mixture was separated by chromatography. Two rhodium(III) products were obtained, the anticipated monomer [Rh(*C*,*C*′-im-py)(Ph_3CCO_2)I_2] (**6**) (30% yield) and [Rh(*C*,*C*′-im-py)((*p*-Ph_3C-C_6H_4)Ph_2CCO_2)I_2] (**7**) (5% yield). No dimers were found. The (*p*-Ph_3C-C_6H_4)$Ph_2CCO_2^-$ carboxylate ligand is new and the intermediate (*p*-Ph_3C-C_6H_4)Ph_2C^- carbanion presumably formed when trityl chloride was treated with excess sodium through coupling of the trityl radical to afford Gomberg's dimer followed by reduction of this species.[11] Although the results suggest sterically bulky carboxylates significantly repress the formation of the dimeric rhodium(II) species, this is at the cost of lower yield and markedly longer reaction times.

ESI-MS Spectrometry. The positive-mode electrospray ionization mass spectrometry (ESI-MS) spectra are briefly mentioned here as the results become important for the discussion of the redox chemistry of the rhodium complexes (see below). The (+)-ESI-MS spectra of the monomers **3** and **5**−**7** aspirated in acetonitrile solution are essentially the same: they show only a single strong envelope of peaks centered at *m*/*z* 697.4 for the [Rh(*C*,*C*′-im-py)I_2(MeCN)]$^+$ ion (calcd. *m*/*z* 697.9). In contrast, the spectra of dimers **4-*anti*/*syn*** show a strong envelop of peaks corresponding the [Rh_2(*C*,*C*-im-py)$_2$(OAc)$_2$I]$^+$ ion at *m*/*z* 1051.1 (calcd. *m*/*z* 1051.1). The monomers **3** and **5**−**7** loose the carboxylate ligand in the ionization process, not an iodo ligand, whereas the converse is true of the dimers **4-*anti*/*syn***.

NMR Spectroscopy: Pyridin-2-yl Zwitterion or Pyridin-2-ylidene NHC? The *C*-metalated pyridinium ligand has been described both as a zwitterion and as a "normal" *N*-heterocyclic carbene.[12] Scheme 3 illustrates these mesomeric extremes and highlights the analogy and distinction between conventional imidazolium-derived NHCs and 2-pyridinium-derived NHCs. Complexes **2**−**7** introduce a novel chelate ligand in which both the imidazolylidene-NHC and the pyridinium-derived donors coordinate to the same rhodium(III)/(II) center. Within each of **2**−**4**, **6**, and **7**, the coordination environments of the imidazolylidene-NHC and pyridinium-derived donors are identical thus facilitating a direct comparison between them.

Scheme 4. "Conventional" *C*(2)-imidazolylidene versus *C*(2)-pyridylidene *N*-heterocyclic Carbene Donors

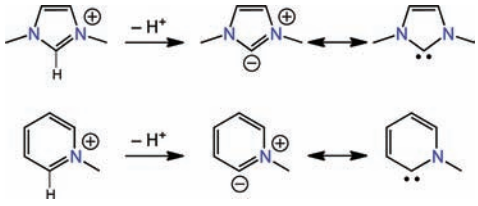

The NMR spectra of **2**−**7** are indicative of bis(carbene) rhodium complexes. All requisite signals are observed in the ^{1}H spectra and, for **2**−**4**, in the $^{13}C\{^1H\}$ NMR spectra for each complex. Data for carbene donor atom signals from the $^{13}C\{^1H\}$ NMR spectra are presented in Table 1, as well as data for representative rhodium(III) complexes with imidazolylidene-NHC and pyridylidene-NHC ligands taken from the literature.[13,14] HMQC- and HMBC-NMR experiments allowed for unambiguous assignment of the carbene carbon signals. The signals at higher chemical shifts with lower coupling constants

dx.doi.org/10.1021/ic202164v | *Inorg. Chem.* 2012, 51, 2191−2203

Table 1. ^{13}C NMR Data for the Carbene Carbon Atom

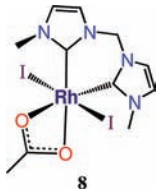

8

complex	δ ^{13}C (CH_3CN) for C_{NHC}	^1J $^{13}C-^{103}Rh$ (Hz)
1 [8]	186.1 (C_{im})	49
2	175.83 (C_{py})	36.9
	162.03 (C_{im})	40.9
3	183.65 (C_{py})	34.6
	167.72 (C_{im})	41.7
4-*anti*	195.24 (C_{py})	57.9
	167.72 (C_{im})	52.6
$[Rh^{III}(C,C'\text{-im}\sim\text{im})(OAc)I_2]$[13] (**8**)	151.34	42.4
$[Rh^{I}Cl(1,5\text{-cyclooctadiene})(2\text{-}(1\text{-methylpyridylidene}))]$[14]	216.6 (in $CDCl_3$)	43

Table 2. Crystal and Structure Determination Data for Complexes 2–4 and 7

	2·$2H_2O$	**3**·CH_2Cl_2	**4-*anti***·$4CH_2Cl_2$	**4-*syn***·$0.5CH_2Cl_2$·$1.5H_2O$	**7**·CH_3CN
formula	$C_{17}H_{30}F_6I_2N_4O_5PRh$	$C_{20}H_{29}Cl_2I_2N_4O_3Rh$	$C_{42}H_{56}Cl_8I_2N_8O_6Rh_2$	$C_{38.50}H_{54}ClI_2N_8O_{7.50}Rh_2$	$C_{58}H_{56}I_2N_5O_3Rh$
crystal system	monoclinic	monoclinic	monoclinic	monoclinic	triclinic
space group	$P2_1/c$	$P2_1/c$	$P2_1/c$	$P2_1/c$	$P\bar{1}$
a, (Å)	15.3957 (16)	15.7153 (11)	15.846 (2)	15.706 (3)	10.5255 (11)
b, (Å)	11.599 (1)	13.9863 (9)	27.020 (3)	13.5868 (17)	13.6554 (16)
c, (Å)	17.6253 (19)	12.4599 (7)	14.0385 (18)	23.595 (4)	19.825 (3)
α (deg)	90	90	90	90	102.685 (5)
β (deg)	111.906 (3)	97.427 (3)	102.645 (3)	91.592 (4)	96.435 (5),
γ (deg)	90	90	90	90	110.518 (3)
V (Å^3)	2920.2 (5)	2715.7 (3)	5865.0 (12)	5033.3 (14)	2547.2 (5)
Z	4	4	4	4	2
μ (mm^{-1})	2.83	3.13	2.03	1.99	1.6
T_{min}, T_{max}	0.586, 0.915	0.328, 0.859	0.790, 0.945	0.764, 0.971	0.794, 0.952
no. of measured, independent, and observed $[I > 2\sigma(I)]$ reflections	18306, 5131, 2456	15734, 4697, 3379	42800, 10238, 5167	15691, 8437, 3113	28342, 8960, 4263
R_{int}	0.116	0.06	0.162	0.147	0.111
$R[F^2 > 2\sigma(F^2)]$, $wR(F^2)$, S	0.053, 0.179, 0.86	0.035, 0.122, 0.78	0.066, 0.193, 0.89	0.084, 0.246, 0.95	0.053, 0.131, 0.98
no. of reflections	5131	4697	10238	8437	8960
no. of parameters	386	296	629	539	629
no. of restraints[a]	97	0	14	3	21
$\Delta\rho_{max}$, $\Delta\rho_{min}$ (e Å^{-3})	0.79, −0.73	0.85, −0.73	1.60, −1.21	1.64, −0.93	0.94, −0.86

[a]See Supporting Information for details.

Table 3. Selected Rhodium–Ligand Bond Lengths (Å) and Inter-Bond Angles (deg)

	Rh–C_{im}	Rh–C_{py}	Rh–Rh	C_{im}–Rh–C_{py}	C_{im}–Rh–L^{trans}	C_{py}–Rh–L^{trans}
2	1.934(13)	1.985(13)		79.8(5)	175.1(4)	176.8(5)
3	1.921(6)	1.953(7)		77.8(3)	167.4(2)	174.5(2)
4-*anti*	1.922(12), 1.946(14)	1.978(13), 1.961(13)	2.6204(13)	80.2(5), 79.8(5)	175.8(4), 175.8(4)	175.4(4), 172.9(4)
4-*syn*	1.940(20), 1.956(19)	1.946(17), 1.984(17)	2.594(2)	80.0(8), 79.1(7)	176.7(7), 176.7(6)	175.5(7), 175.0(6)
7	1.952(9)	1.983(9)		78.3(4)	166.5(3)	174.9(3)

are attributed to the pyridylidene carbene carbon. The ^1J $^{13}C-^{103}Rh$ coupling constants are similar to those reported for analogous Rh–C_{im} and Rh–C_{py} complexes. The assignment of the metalated pyridinium ring as a normal pyridylidene carbene is consistent with the detailed NMR and structural studies with bonding analyses reported by Raubenhiemer and Frenking.[12c–e]

X-ray Crystallography. X-ray crystal structures were obtained for compounds **2**–**4** and **7**. Crystallographic data are presented in Table 2, and key metal–ligand bond lengths and angles for the complexes are listed in Table 3. Brief description for each complex is followed by a description of common features.

*[Rh(C,C′-im-py)(H$_2$O)$_2$I$_2$][PF$_6$] (**2**).* Figure 1 presents a view of the $[Rh(C,C'\text{-im-py})(H_2O)_2I_2]^+$ cation. The rhodium(III) cation exhibits distorted octahedral geometry. The transoid angles I1–Rh–I2, C11–Rh–O1W and C1–Rh–O2W are 178.44(6)°, 175.1(4)°, and 176.8(5)°, respectively.

dx.doi.org/10.1021/ic202164v | Inorg. Chem. 2012, 51, 2191–2203

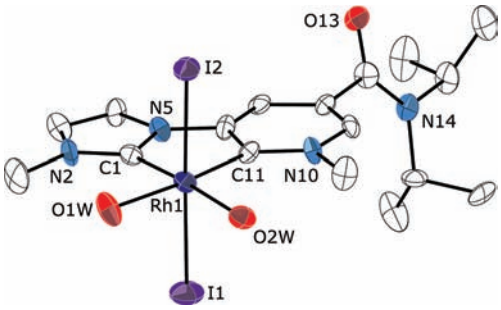

Figure 1. View of the cation from the X-ray crystal structure of $[Rh(C,C'\text{-im-py})(H_2O)_2I_2][PF_6]$ (**2**); 50% thermal ellipsoids at 150 K are shown, and, for clarity, H-atoms are omitted.

The bite angle, C1−Rh−C11, of the *C,C′*-im-py ligand is 79.9(5)°. The Rh−C_{im} bond, 1.934(13) Å, is shorter than the Rh−C_{py} bond, 1.985(13) Å.

*[Rh(C,C′-im-py)(RCO$_2$)I$_2$] (**3**: R = Me, **7**: R = C(p-C$_6$H$_4$−CPh$_3$)Ph$_2$).* The structures of **3** and **7**, Figure 2, are similar to

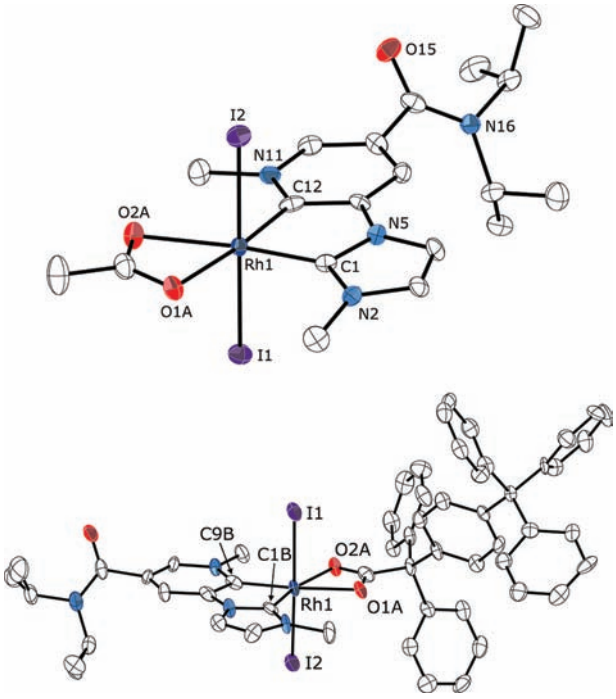

Figure 2. View of the molecular structures from the X-ray crystal structures of **3** and **7**; 50% thermal ellipsoids at 150 K are shown and, for clarity, H-atoms are omitted.

that of **2** in terms of bite, transoid, and in-plane ligand−rhodium−ligand interbond angles and the corresponding rhodium−ligand bond lengths. The Rh−C_{im} bond lengths, 1.934(13) Å in **3** and 1.921(6) Å in **7**, are again shorter than the Rh−C_{py} bond lengths, 1.985(13) Å in **3** and 1.953(7) Å in **7**.

*Syn- and anti-[Rh$_2$(C,C′-im-py)$_2$(OAc)$_2$I$_2$] (**4-anti, 4-syn**).* The isomeric rhodium(II) dimers, **4-*anti***, **4-*syn***, both display two octahedral metal centers co-joined by a Rh−Rh bond. The difference between the isomers is the relative orientation of the two *C,C′*-im-py chelate ligands, which in **4-*anti*** lie antiparallel and in **4-*syn*** lie parallel. The I−Rh bonds in both isomers are not parallel to the Rh−Rh bond, but rather are closer to perpendicular to the plane made by the proximate *C,C′*-im-py ligand (Figure 3). Thus, the Rh−Rh−I bond angles are 173.35(5)° and 170.87(5)° in **4-*anti***, whereas the I−Rh−$C_{carbene}$ bond angles are 83.5(3)°, 91.7(3)°, 89.7(3)°, and 88.1(3)°. The trend is similar in **4-*syn*** with Rh−Rh−I bond angles of 172.57(8)° and 170.5(8)° and I−Rh−$C_{carbene}$ bond angles of 89.3(5)°, 92.6(4)°, 88.7(6)°, and 88.6(5)°. The I−Rh−Rh−I dihedral angles are 12.3° and 39.9° in **4-*anti*** and **4-*syn*,** respectively, and are indicative of the splaying apart of the coordination planes of the two bonded Rh centers. This is due to two factors. First, to accommodate the relatively short Rh−Rh bonds, 2.6204(13) Å in **4-*anti*** and 2.594(2) Å in **4-*syn***, the bridging carboxylates are twisted with respect to each other (Figure 4); the O−Rh−Rh−O dihedral angles for each acetate bridge are 19.9° and 22.5° in **4-*anti*** and 19.8° and 20.9° in **4-*syn***. Twisting of the acetate bridges is observed in analogous $[Rh_2(\text{bis-chelate})_2(\mu\text{-OAc})_2X_2]^{z+}$ (X = Cl, MeCN, pyridine) dimers.[15] Second, the two *C,C′*-im-py ligands in each dimer are rotated with respect to one another, by 30.6° in **4-*anti*** and by 22.6° in **4-*syn***, thereby optimizing offset $\pi-\pi$ stacking. The π-stacked interaromatic ring distances are 3.1−3.3 Å in **4-*anti*** and 3.1−3.8 Å in **4-syn**, indicative of the increased splaying of the *C,C′*-im-py ligands in the *syn*-isomer that decreases the steric interactions between the adjacent bulky bis(iso-propyl)amide substituents.

Common Features. *C,C′-im-py Ligand.* In all of the structures **2**, **3**, **4-*anti/syn***, and **7**, the imidazolylidene and pyridylidene rings within the *C,C′*-im-py ligand are near coplanar; the most twisted *C,C′*-im-py ligands are within the dimers **4-*syn*** (mean inter-ring angle 14.2°) and **4-*anti*** (mean inter-ring angle 8.3°). The *C,C′*-im-py bite angles are relatively consistent, with a mean bite angle of 79.3(2)°.

Rh−C_{NHC} Bond Lengths. The Rh^{II}−C_{NHC} bond lengths in **4-*anti*** and **4-*syn*** show significant variation (see Table 3). The mean Rh−C_{im} bond distances for the Rh(II) dimers, **4-*anti/syn***, and for the Rh(III) monomers, **2**, **3**, and **7**, are not significantly different (1.936(3) and 1.941(4) Å, respectively). Likewise, the mean Rh−C_{py} bond distance in the rhodium(II) dimers (1.967(4) Å) is not significantly different from that of the Rh(III) monomers **2**, **3**, and **7** (1.974(3) Å). Nonetheless, all Rh−C_{im} bonds are shorter than the corresponding Rh−C_{im} bond (2.016(4) Å) in the rhodium(I) complex, **1b**,[8] and the Rh−C_{im} bond lengths are comparable to those found for similar (NHC)Rh^{III} complexes.[10,16] For example, Crabtree and Peris report Rh−C_{im} bond lengths of 1.992(9), 2.000(10)Å for [Rh(III)(1,3-(*N*-butylimidazol-2-ylidene)benzene)(OAc)I_2].[10] The Rh^{III}−C_{py} bond lengths are also similar to those reported for other rhodium complexes with pyridin-2-ylidene ligands in the literature, of which there are only few,[17] for example, [RhCl(COD)(*N*-isopropylisoquinolin-1-ylidene)] has a Rh−C_{py} bond length of 2.024(2).[17c]

Although the Rh−C_{im} and Rh−C_{py} bond lengths do not vary significantly with the oxidation state of rhodium in **2**, **3**, **4-*anti/syn***, and **7**, there is a significant difference between the two types of Rh−C_{NHC} bond lengths within each complex. In every complex, the Rh−C_{im} bond length is shorter than the Rh−C_{py} bond length. The mean difference in the Rh−C_{py} and Rh−C_{im} bond lengths is 0.038(3) Å for the rhodium(III) monomers **2**, **3**, and **7**, and is 0.019(4) Å for the rhodium(II) dimers **4-*anti/syn***. The average C_{NHC}−Rh−L^{trans} bond angle is 174.2(2)°. Reasons for the trends in Rh−C_{NHC} bond lengths are discussed in the section on DFT calculations below.

Redox Chemistry. To ascertain the redox properties of the bound *C,C′*-im-py dicarbene ligand, cyclic voltammograms of **3**

dx.doi.org/10.1021/ic202164v | *Inorg. Chem.* 2012, 51, 2191−2203

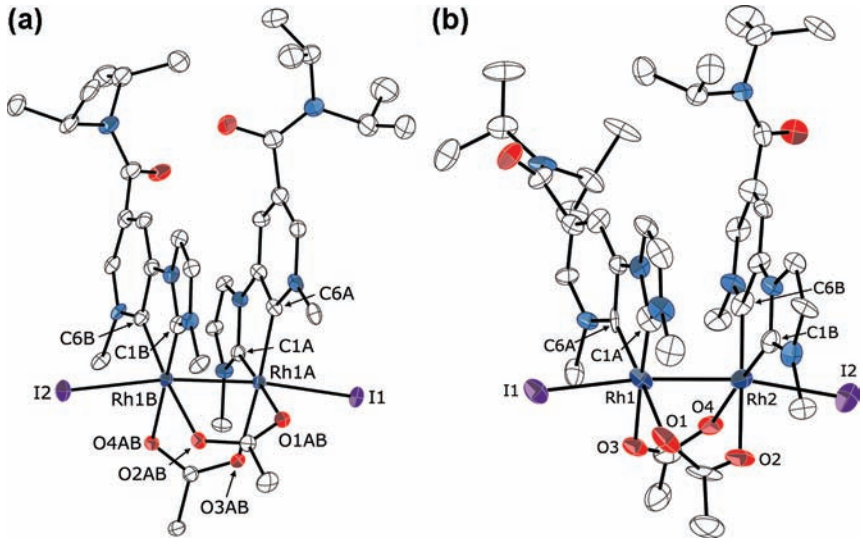

Figure 3. Views from the X-ray crystal structures of the (a) *anti*- and (b) *syn*-isomers of $[Rh_2(C,C'\text{-im-py})_2(OAc)_2I_2]$ (**4-*anti*, 4-*syn***); 50% thermal ellipsoids at 150 K are shown and, for clarity, H-atoms are omitted.

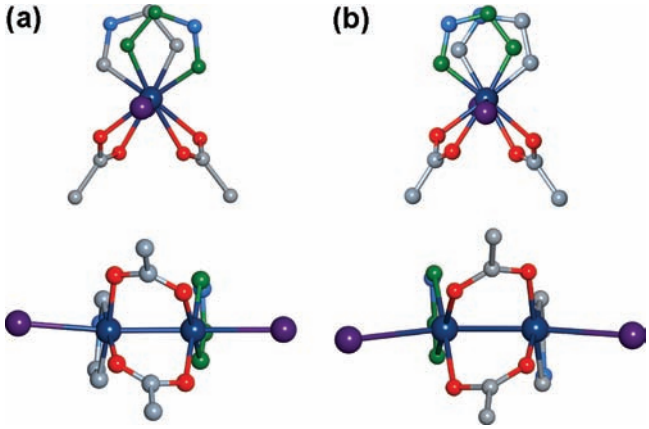

Figure 4. Comparison of the coordination environments for the (a) *anti*- and (b) *syn*-isomers of $[Rh_2(C,C'\text{-im-py})_2(OAc)_2I_2]$ (**4-*anti*, 4-*syn***); C-atoms on different *C,C'*-im-py ligands are colored green and gray.

and, to help with assignment of redox processes, those of the congeneric bis(imidazolylidene)rhodium(III) complex **8**,[13] and of dimers **4-*anti/syn*** were recorded in acetonitrile. Except where explicitly stated otherwise, the potentials cited below are all against an Ag/AgCl reference electrode for which $E_{1/2}$ (ferrocenium/ferrocene) = +0.49 V.

The cyclic voltammograms of **3**, Figure 5(a, b), reveal a sharp, chemically irreversible reduction at −1.07 V [$E_p - E_{p/2}$ = 45 mV cf. ΔE_p ($Fc^{+/0}$) = 70 mV at 100 mV s^{-1} scan rate]. Comparison of the cathodic current and the $E_p - E_{p/2}$ values for the irreversible reduction with the other peaks in the cyclic voltammograms, and with those in cyclic voltammograms with ferrocene standard, suggests the reduction corresponds to a two-electron Rh(III) to Rh(I) process. In return anodic sweeps after scanning through the −1.07 V reduction, a broad triplet of peaks rises at about +0.45 to +0.8 V. These peaks are more prominent at faster scan rates (500 mV s^{-1} or greater). The two peaks at +0.65 and 0.85 V, indicated by the markers in Figure 5, are attributable to the I^-/I_3^- and I_3^-/I_2 couples,[18] respectively (see also Figure 6). This behavior indicates iodide ion is not originally present in solution, but is a product of the Rh-centered reduction at −1.07 V. Consistent with this conclusion, ESI-MS revealed that loss of acetate ion, not iodide ion, is the principle ionization pathway for **3** (see above). Scans to extended potentials reveal additional processes: a quasi-reversible reduction process at −1.85 V and a broad, electrochemically irreversible oxidation process at +1.55 V ($E_p - E_{p/2}$ = 180 mV) followed by a second quasireversible process at about +1.8 V (ΔE_p = 120 mV) in the tail of the anodic solvent discharge. The assignment of these processes is assisted by comparison with the redox behavior displayed by **8**.

Cyclic voltammograms of complex **8**, for example, Figure 5c, exhibit a sharp, chemically irreversible reduction process at −0.96 V ($E_p - E_{p/2}$ = 35 mV) that gives rise in reverse sweeps to an overlapping pair of broad anodic peaks at −0.34 and −0.07 V corresponding to oxidation of product(s) from the reduction process. The current and width of the −0.96 V reduction peak are indicative of a two-electron Rh(III) to Rh(I) process. The similarity of the potentials for the Rh(III)−Rh(II) reduction suggests a similar donor ability for the *C,C'*-im∼im chelate in **8** and for the *C,C'*-im-py chelate in **3**. In cyclic voltammograms for **8**, peaks at +0.65 and +0.85 V corresponding to oxidation of free iodide ion were observed at faster scan rates (≥500 mV s^{-1}) for **8**. In scans to positive potential are an irreversible oxidation at +1.53 V and a partially reversible couple +1.73 V (ΔE_p = 120 mV), respectively.

Overall, the electrochemistry displayed by complex **8** is very reminiscent of that for **3**, with only one, but notable, exception: the quasi-reversible reduction process at about −1.85 V for **3** is missing in cyclic voltammograms of **8**. The common processes for **3** and **8** must be centered at the conserved $[Rh^{III}\{C_{NHC}\sim C'_{NHC}\}I_2(OAc)]$ core: By elimination, therefore, the reduction couple at −1.85 V for **8** (and for **4-*anti/syn***, see below) may be attributed to one-electron reduction of the Rh-bound *C,C'*-im-py ligand. The corresponding "free" pyridinium cation, $[Him\text{-}pyH]^{2+}$, shows a two-electron reduction peak at −0.75 V.[8] Although the low potential for reduction of the bound *C,C'*-im-py ligand compared to that for $[Him\text{-}pyH]^{2+}$ is suggestive for decreased electron acceptor ability upon *C*-metalation of the pyridinium ring (carbene formation), it is difficult to discern whether this is principally due to the change in the charge or the electronic structure of the ring.

dx.doi.org/10.1021/ic202164v | *Inorg. Chem.* 2012, 51, 2191−2203

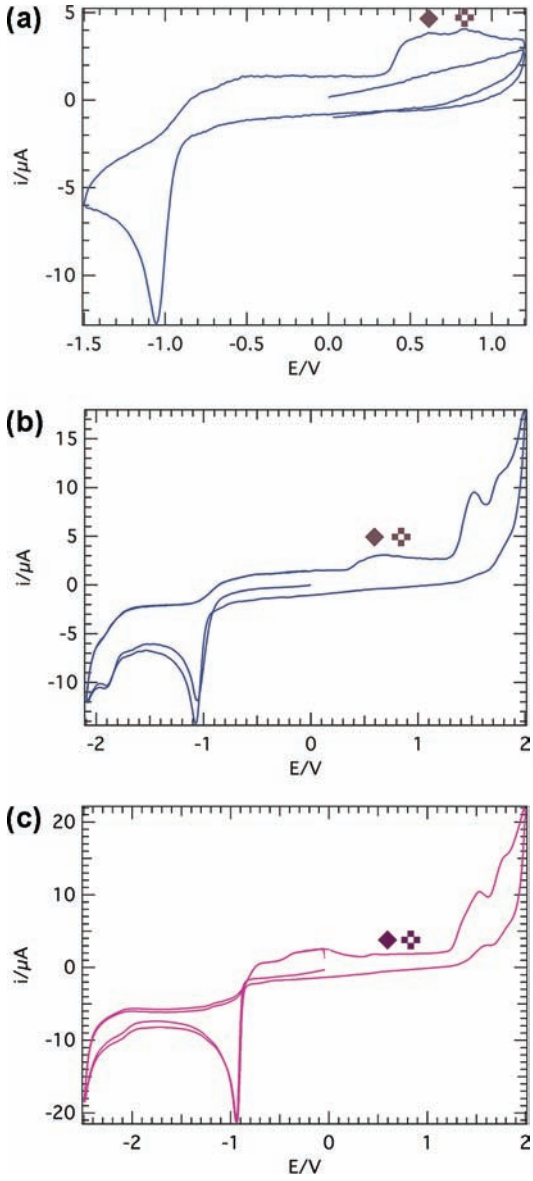

Figure 5. Cyclic voltammograms of [Rh(*C,C′*-im-py)(OAc)I_2] (**3**) (a and b) and [Rh(*C,C′*-im~im)(OAc)I_2] (**8**) (c). Conditions: 0.1 M [(*n*-Bu)$_4$N][PF_6] in acetonitrile at 295 K; glassy carbon mini-disk (0.5 mm diameter) working electrode; scan rate = 100 mV s^{-1}; $E_{1/2}$(ferrocenium/ferrocene) = +0.47 V. The peak potentials for the I^-/I_3^- (magenta filled diamonds) and I_3^-/I_2 (magenta filled crosses) couples are indicated.

UV−vis spectra acquired upon electrolysis of **3** at −1.0 V in a thin-layer spectro-electrochemical cell are shown in Figure 6. Clean conversion of **3** with peaks 264, 331, and 419 nm[19] (ε = 3.19 × 10^4, 2.60 × 10^4, and 1.71 × 10^3 M^{-1} cm^{-1}, respectively) to a species with bands at 243, 334, and 382 nm (ε = 3.40 × 10^4, 8.96 × 10^3, and 7.15 × 10^3 M^{-1} cm^{-1}, respectively) with isosbestic points at 253, and 353 nm was observed. No peaks were observed in the long, low-energy tail, including upon repetition of the electrolysis experiment employing a higher concentration of **3**. The post-electrolysis product was EPR silent. In UV−vis spectra, a pyridinium cation usually exhibits a band at ~290 nm whereas dihydropyridines typically show bands at ~260 and ~330 nm.[8,20] Thus, the UV−vis spectra of the product (peaks at 243 and 334 nm) are not inconsistent with a dihydropyridine center, but the comparison of the cyclic

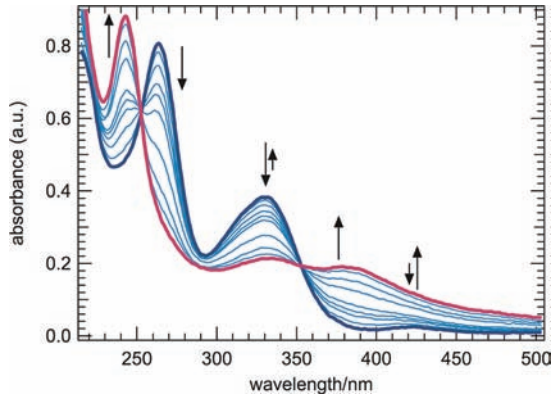

Figure 6. Changes in the UV−vis spectra accompanying reduction of [Rh(*C,C′*-im-py)(OAc)I_2] (**3**); arrows mark the direction of change.

voltammetry of **3** with that of **8** suggests a Rh-centered process occurs (see above). This was confirmed by UV−vis spectroelectrochemistry, which exhibits conversion of **8** with peaks at 272 and 343 nm (ε = 3.24 × 10^4 and 1.43 × 10^4 M^{-1} cm^{-1}) to a reduction product with peaks at 243, 347, and 408 nm (ε = 3.74 × 10^4, 6.11 × 10^3, and 2.28 × 10^2 M^{-1} cm^{-1}, respectively); see Supporting Information. The identities of the (presumably Rh(I)) reduction products of **3** and **8** are currently being investigated.

Cyclic voltammograms of **4-*anti*** are presented in Figure 7a,b. Cyclic voltammograms of isomeric **4-*syn*** were also recorded (see Supporting Information) and are indistinguishable from those of **4-*anti***. To negative potentials, the cyclic voltammograms are dominated by a broad reduction process at E_p = −1.21 V (E_p − $E_{p/2}$ = 150 mV) that gives rise to a coupled broad anodic peak at E_p = −0.64 V in the reverse sweep. There are two possibilities for the redox behavior underlying the broad reduction couple: (i) reductive breakup of Rh(II) dimer to afford monomeric Rh(I) species, as is exemplified by [Rh(dppm)$_2$Cl$_2$(OAc)$_2$] (dppm = bis(diphenylphosphino)-methane),[15d] or (ii) reductive aggregation of the Rh(II) dimers to afford, initially, mixed-valent Rh_4^{3+} and Rh_4^{2+} tetramers and, eventually, mixed-valent Rh(I)−Rh(II) molecular wires, as exemplified by [Rh(diimine)(RCO$_2$)]$_2^{2+}$ dimers upon reduction.[21] In both cases, a broad cathodic peak is anticipated because the kinetics of the electron transfer are inhibited by the concerted structural changes inherent to the reduction of Rh(II) centers. We return to the assignment of the broad reduction couple after presenting spectroelectrochemical results (see below). To positive potentials in the cyclic voltammograms of dimers **4**, peaks for the I^-/I_2 and I_3^-/I_2 couples are present in the first sweep (i.e., before the reduction process at −1.21 V is traversed) and the current of these peaks remains unchanged upon scanning through the reduction process(es). Thus, it may be concluded that the iodo ligand is replaced by acetonitrile, which concurs with the mass spectrometry results (see above). In scans to extended potentials, the cyclic voltammograms of **4-*anti/syn*** show quasi-reversible couples at −1.85 V and at +1.55 V. Following the same reasoning as given for **3** (see above), the −1.85 V couple may be attributed to a one-electron reduction centered on each Rh-bound *C,C′*-im-py ligand.

UV−vis spectra acquired early in the electrolysis of **4-*anti*** at −1.4 V are presented in Figure 8. Upon reduction, the UV−vis bands for **4-*anti*** at 240, 288, and 375 nm (ε = 3.60 × 10^4, 1.12 × 10^4, and 1.68 × 10^4, respectively) were cleanly replaced by

dx.doi.org/10.1021/ic202164v | *Inorg. Chem.* 2012, 51, 2191−2203

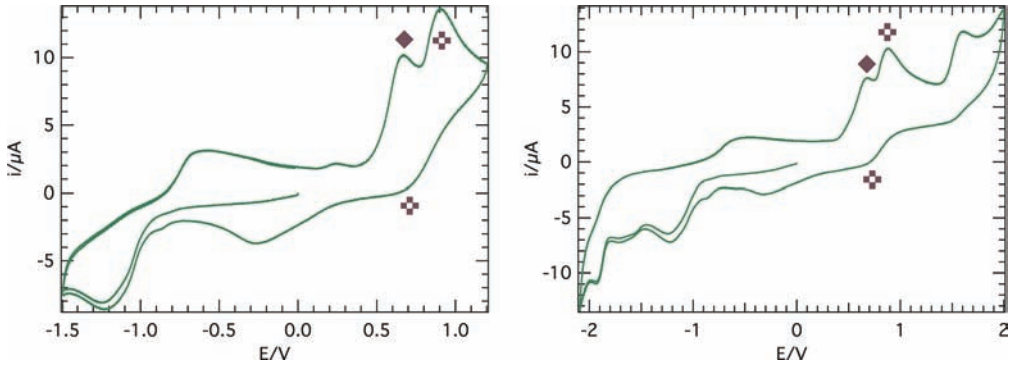

Figure 7. Cyclic voltammograms of *anti*-$[Rh_2(C,C'\text{-im-py})_2(OAc)_2I_2]$ (**4-*anti***). Conditions as for Figure 5.

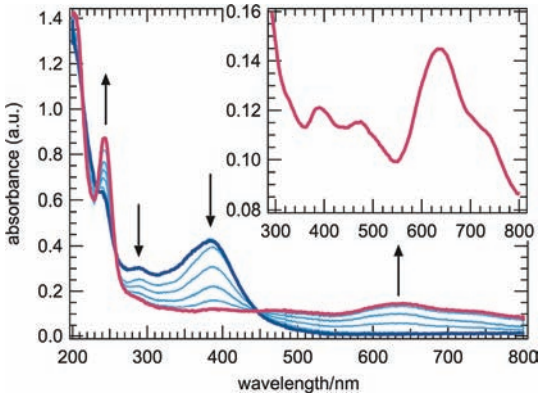

Figure 8. Changes in the UV−vis spectra accompanying reduction of *anti*-$[Rh_2(C,C'\text{-im-py})_2I_2(OAc)]$ (**4-*anti***); arrows mark the direction of change and the inset shows an expansion of the final spectrum.

those for a new species with a sharp peak at 245 nm ($\varepsilon = 4.9 \times 10^4$ M^{-1} cm^{-1}) and a broad absorbance through the visible region with a prominent peak at 636 nm ($\varepsilon = 8.2 \times 10^3$ M^{-1} cm^{-1}) and weaker peaks at 388, 470 and ~730 nm ($\varepsilon = 6.9 \times 10^3$, 6.7×10^3, and 6.5×10^3 M^{-1} cm^{-1}, respectively) (see the inset to Figure 8); isosbestic points were observed at 235, 257, and 447 nm. The product was EPR silent, suggesting that it is diamagnetic. The UV−vis spectrum of the product is almost identical in profile to that displayed by the molecular wire $[Rh_2(\mu\text{-}OAc)_2(phen)_2]_n^{n+}$ upon dissolution in dimethylformamide (dmf), which shows an intense band at 590 nm and weaker bands at ~450 and ~770 nm.[21b,e] Chardon-Noblat, Pruchnik, and co-workers demonstrated that $[Rh_2(\mu\text{-}OAc)_2(phen)_2]_n^{n+}$ is comprised of Rh(I)−Rh(II) mixed-valent $[Rh_2(\mu\text{-}OAc)_2(phen)_2]_2^{2+}$ tetramers linked into an infinite wire by Rh−Rh bonding; it is the diamagnetic tetramer that is observed in dmf solution.[21b] Therefore, we assign the reduction of **4-*anti*** at −1.21 V to reductive tetramer formation, eq 1:

$$2[Rh_2(C,C'\text{-im-py})_2(\mu\text{-}OAc)_2(MeCN)_2]^{2+} + 2e^- \rightleftharpoons [Rh_2(C,C'\text{-im-py})_2(\mu\text{-}OAc)_2(MeCN)]_2^{2+} + 2MeCN \quad (1)$$

As **4-*anti*** remains soluble upon reduction, molecular wires of linked tetramer do not form. Significantly, the profile of the reduction couple with its distinct asymmetry is the same as that observed by Dunbar, Christou, and co-workers[22] and by Chardon-Noblat, Pruchnik, and co-workers[21b] for reduction of the dimers $[Rh_2(\mu\text{-}OAc)_2(L)_2]^{2+}$ (L = various bpy and phen derivatives). This adds confidence to the assignment of eq 1 to the primary reduction of **4-*anti***.

The reduction of **4-*anti***, eq 1, throws light on the debate over whether reduction of the dimers $[Rh_2(\mu\text{-}OAc)_2(L)_2]^{2+}$ (L = various bpy and phen derivatives) is metal- or diimine chelate-centered.[21,22] If our assignment of the −1.85 V process to reduction of the Rh-bound *C,C'*-im-py ligand is correct, as we believe it is, then the reduction at −1.21 V must be rhodium-centered and, therefore, $[Rh_2(C,C'\text{-im-py})_2(\mu\text{-}OAc)_2(MeCN)]_2^{2+}$ and, by comparison, $[Rh_2(\mu\text{-}OAc)_2(L)_2]_n^{n+}$ are $Rh^I\text{^}Rh^{II}-Rh^{II}\text{^}Rh^I$ species (where "^" indicates a carboxylate-bridged Rh−Rh bond) as argued by Chardon-Noblat, Pruchnik, and co-workers.[21]

Chemical Reduction of Monomer 3. Reactions of **3** with several reagents capable of reducing pyridinium salts to the corresponding dihydropyridines, including dithionite ion (two phase water−dichloromethane system), $NaBH_4$, $LiBH(sec\text{-}butyl)_3$, $NaBH(OAc)_3$ were attempted. $KBH(sec\text{-}butyl)_3$ is known to reduce metal-bound pyrimidylidene ligands to their corresponding dihydropyrimidylidene analogues.[23] In all these reactions of **3**, complete decomposition and no evidence of any dihydropyridine product was observed. This is consistent with reduction of the metal-bound *C,C'*-py~im ligand being thermodynamically difficult (one-electron reduction is at −2.34 V vs Fc^+/Fc, see above). Thus, the rhodium center is reduced and the product(s) quickly decomposes.

Hydride addition to *C*-metalated 6-membered *N*-heterocyclic ligands is known. Cabeza et al. found that pyrimidylidene-bridged ruthenium−carbonyl clusters $[Ru_3(\mu\text{-}H)(\mu\text{-}\kappa^2N^1,C^6\text{-}pymMe)(CO)_{10}]$ (H-pymMe$^+$ = *N*-methylpyrimidinium cation) and $[Ru_3(\mu\text{-}H)(\mu\text{-}\kappa N^1,C^2\text{-}pymMe)(CO)_{10}]$ (and related analogues) react with $KBH(sec\text{-}butyl)_3$ to give the corresponding ruthenium cluster-bound dihydropyrimidylidene products.[23b,c] However, cyclic voltammetry revealed that the reduction of the *C*-metalated *N*-pyrimidinium ligands occurred at considerably higher potential (−0.70 to −1.00 V vs SCE, $Fc^{0/+}$ = 0.59 V) than we observe for the *C,C'*-im-py ligand and was the first reduction process to occur in each ruthenium complex. Similarly, Tanaka et al. report that the primary reduction of $[(bpy)Ru(pad)]^{2+}$ (pad = 2-(2-pyridyl)acridine) at −1.10 V (vs. SCE) in acetonitrile−water affords the corresponding dihydroacridine complex, $[(bpy)Ru(padH_2)]^{2+}$.[24] A condition for successful hydride addition to a *C*-metalated 6-membered *N*-heterocyclic ligand thus appears to be that the primary reduction process for the complex is centered on this ligand. The energetics of hydride addition to **1**−**3** and related complexes were further probed by DFT calculations.

dx.doi.org/10.1021/ic202164v | *Inorg. Chem.* 2012, 51, 2191−2203

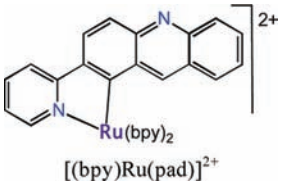

DFT Calculations. *Structure.* The minimized structures of **1b**, **2**, and **3** obtained from DFT calculations show excellent fidelity with the structures for these species determined by X-ray crystallography; for example, see Table 4. In particular, the Rh−C_{NHC} bond distances in the calculated structures mirror those of the experimentally determined structures. Slightly shorter calculated over experimental M−X (X = halogen) distances were found in other studies of transition metal−pyridylidene species.[12c−e] The consistency between calculation and experiment provides confidence in the calculations.

As the coordination environments of the carbene carbons, C_{im} and C_{py}, are identical in **1**−**4** and **7**, the Rh−C_{NHC} bond lengths observed in the crystal structures (see above) should be diagnostic of the respective bond strengths. Thus, the consistently shorter Rh−C_{im} bond lengths suggest the imidazolylidene donor forms a stronger Rh−C_{NHC} bond than does the pyridylidene donor. This contradicts the expectation that less stabilized carbenes, those with less heteroatoms or with heteroatoms further from the carbene carbon, should bind more strongly to a metal.[12] A possible reason is that the different ring sizes in the rigid *C,C′*-im∼py chelate ligand result in different intramolecular steric interactions with the flanking *N*-bound methyl groups as depicted in Scheme 5. We probed this by comparing the Rh−C_{NHC} bond lengths from the minimized structures calculated for complex **3** and a hypothetical analogue **3(Me→H)** in which the flanking methyl groups are replaced by hydrogen atoms. At the M06-L/def2-SVP level of theory, for **3** Rh−C_{im} (1.930 Å) is shorter than Rh−C_{py} (1.958 Å) (Table 3), whereas for **3(Me→H)** the trend reverses: Rh−C_{im} (1.941 Å) is longer than Rh−C_{py} (1.928 Å) (Supporting Information, Table S3). The result is independent of the level of theory employed (Supporting Information, Table S3) and confirms the importance of the different intramolecular steric interactions imposed by the imidazolylidene and pyridylidene rings.

Scheme 5

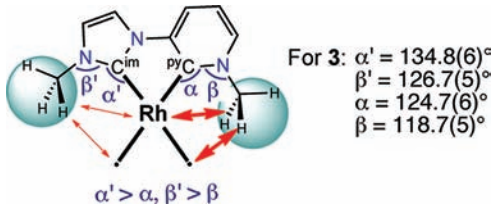

Addition of Hydride Ion to the Pyridinium Ring. The DFT calculations predict only minor structural changes upon hydride addition to the 4-position of the pyridinium ring, be it nonmetalated as in **1b** or metalated as in **2** or **3**. Only two structural changes upon hydride addition are noteworthy: First, the C(3)−C(4)−C(5) bond angle in the pyridinium ring drops from about 118° to about 108° consistent with the change from a sp^2 to sp^3 C(4)-carbon atom. Second, for the species with a rhodium-bound *C,C′*-im-py ligand, the Rh−C_{py} bond lengthens from about 1.96 to 2.00 Å, suggesting a loss of bond strength. Overall, there is no steric impediment to hydride addition.

Results from calculations of the ^{13}C chemical shifts and the ^1J ^{13}C-^{103}Rh coupling constants for [Rh(*C,C′*-im-py)(OAc)-I_2(MeCN)]$^{2+}$, the solvato-species formed by exchange of the aqua ligands in **2** with solvent, and the hypothetical adduct formed by hydride addition to [Rh(*C,C′*-im-py)(OAc)-I_2(MeCN)]$^{2+}$ are also presented in Table 4. Accurate DFT prediction of NMR parameters of ligands attached to heavy transition metals is difficult,[25] and it is no surprise that despite incorporating spin−orbit coupling and employing all-electron basis sets in the calculations, the calculated chemical shifts for the carbene carbon atoms are consistently low (by ∼5−8% relative to TMS) compared to the experimental values. The calculated shifts for the ring carbons improve further away from

Table 4. Calculated[a] and Observed Structural and NMR[b] Parameters for Complexes 2 and 3 and Their Hydride Adducts

	[Rh(*C,C′*-im∼py)-$(H_2O)_2I_2$]$^+$ (**2**)		[Rh(*C,C′*-im∼pyH^4)-$(H_2O)_2I_2$] **2** (+ H^-)	[Rh(*C,C′*-im∼py)-$(OAc)I_2$] (**3**)		[Rh(*C,C′*-im∼pyH^4)-$(OAc)I_2$]$^-$ **3** (+ H^-)
	DFT	Obs'd	DFT	DFT	Obs'd	DFT
Rh−C_{im} (Å)	1.941	1.931(14)	1.930	1.930	1.921(6)	1.930
Rh−C_{py} (Å)	1.973	1.980(14)	2.005	1.958	1.953(7)	2.005
Rh−O (Å)	2.288, 2.294	2.183(9), 2.207(9)	2.250, 2.250	2.213, 2.193	2.155(5), 2.194(5)	2.250, 2.250
Rh−I (Å)	2.699, 2.708	2.6242(15), 2.6480(14)	2.744, 2.742	2.742, 2.736	2.6298(7), 2.6384(7)	2.744, 2.742
C−Rh−C (deg)	79.4	80.3(6)	77.6	78.5	77.8(3)	77.6
I−Rh−I (deg)	174.9	178.48(6)	180.0	177.6	177.99(3)	180.0
C_{im}−Rh−O_{trans} (deg)	175.6	176.2(5)	168.4	168.4	167.4(2)	168.4
C_{py}−Rh−O_{trans} (deg)	178.3	175.3(5)	172.6	172.7	174.5(2)	172.6
C^3_{py}−C^4_{py}−C^5_{py} (deg)	118.4	115.6(12)	108.5	118.4	118.1(6)	108.5
δ (^{13}C) C_{im}	170.0[c]	162.03	165.2[c]			
^1J $^{13}C_{im}$−^{103}Rh (Hz)	48.1[c]	40.9	−46.0[c]			
δ (^{13}C) C_{py}	189.5[c]	175.83	151.2[c]			
^1J $^{13}C_{py}$−^{103}Rh (Hz)	41.1[c]	36.9	−38.1[c]			

[a]Geometries optimized in vacuum using Gaussian09 at the M06-L/def2-SVP level of theory; NMR parameters calculated using the ADF 2010.02 package, two-component ZORA (spin−orbit)/ COSMO acetonitrile solvent; Chemical shifts: SAOP/TZP. Spin−spin couplings: revPBE/TZ2P. [b]For NMR spectra obtained in acetonitrile solution. [c]Values assume water−acetonitrile solvent exchange; that is, they are calculated for [Rh(*C,C′*-im∼py)$(MeCN)_2I_2$]$^+$.

dx.doi.org/10.1021/ic202164v | *Inorg. Chem.* 2012, 51, 2191−2203

the site of metalation. We note the following points: First, exchange of the aqua ligands in **2** to afford $[Rh(C,C'\text{-im-py})(OAc)I_2(MeCN)]^{2+}$ is predicted to have only a small influence on the NMR parameters associated with the bound carbene carbon atoms. Second, for **2**, the ^{13}C chemical shift of C_{py} is calculated to be higher than that of C_{im} by 19.5 ppm, close to the experimental chemical shift difference of 13.7 ppm. The ^{13}C chemical shift of C_{py} is predicted to drop by ~48 ppm following hydride addition to the pyridylidene ring. This is consistent with a reduction in the amount of carbene character for this carbon upon hydride addition, since carbenes are associated with deshielded ^{13}C NMR chemical shifts in general. Third, the ^1J ^{13}C-^{103}Rh coupling constants are predicted to be insensitive to hydride addition (changes are <10%).

We also calculated the energies for hydride addition to the rhodium(I) complex **1a**, to the rhodium(III) complexes **2** and **3**, and, for comparison, to the *N*-methyl-*N*′,*N*′-di(*iso*-propyl)-nicotinamide cation ($\mathbf{9}^+$) and a number of hypothetical rhodium complexes. To minimize systematic errors, the results are presented as electronic energies, corrected for zero-point vibrational energy, for the isodesmic transfer of hydride from the dihydropyridine H-**9** to the species of interest, eq 2, in acetonitrile solution; conclusions are drawn only from these data. The relevant data are presented in Table 4.

$$[Rh(C\text{-im}\sim(pyH^+/C'\text{-py}))X_xY_y]^{z+} + \text{H-}\mathbf{9} \rightarrow [Rh(C\text{-im}\sim(pyH_2/C'\text{-pyH}))X_xY_y]^{(z-1)+} + \mathbf{9}^+ \quad (2)$$

From the results of the DFT calculations, irrespective of the level of theory employed, three significant results can be discerned:

First, transfer of hydride from H-**9** to rhodium species bound by the *C*-im-pyH$^+$ ligand, in which the pyridinium ring is not metalated, is energetically favorable in all cases. The hydride transfer reaction energies depend on the coligands and the oxidation state of the rhodium ion, but without a clear trend. For example, hydride transfer to $[Rh^{III}(C\text{-im-pyH}^+)(H_2O)_2I_2Cl]^+$ is more favorable than to $[Rh^{I}(C\text{-im-pyH}^+)(H_2O)_2Cl]^+$ by 58 kJ mol^{-1}, whereas hydride transfer to $[Rh^{III}(C\text{-im-pyH}^+)(OAc)I_2(ethylene)]^+$ is less favorable than to $[Rh^{I}(C\text{-impyH}^+)(OAc)(ethylene)]^+$ by 7 kJ mol^{-1}.

Second, hydride transfer from H-**9** to all rhodium species bound by the *C*,*C*′-im-py ligand with a *C*-metalated pyridinium ring is always energetically uphill. Uniformly, hydride transfer to a rhodium(I) species is more unfavorable than to a rhodium(III) species. This result is independent of the overall charge on the rhodium complex; for example, hydride transfer from H-**9** to $[Rh^{I}(C,C'\text{-im-py})(OAc)]^+$ is less favorable than to $[Rh^{III}(C,C'\text{-im-py})(I)_2(OAc)]^0$ by 55 kJ mol^{-1}. Clearly, the rhodium oxidation state has a significant effect on the thermodynamics of hydride transfer to the pyridyl ring.

Third, the charge of a species has a much smaller influence on the energetics of the hydride transfer reaction than does metalation of the pyridinium ring. Nonetheless, for species with comparable coordination environments, transfer of hydride is always easier to the more highly charged species; for example, hydride transfer to $[Rh^{III}(C,C'\text{-im-py})(H_2O)_2I_2]^+$, although uphill compared to $\mathbf{9}^+$ by 54 kJ mol^{-1}, is more favorable than to $[Rh^{III}(C,C'\text{-im-py})(OAc)I_2]$ by 20 kJ mol^{-1}.

Table 5. Calculated Energies (kJ mol^{-1})[a] for the Isodesmic Transfer of Hydride from *N*-methyl-*N*′,*N*′-di(*iso*-propyl)dihydronicotinamide (H-9) to the Listed Species in Acetonitrile Solution (ε_r = 37.5)

	ΔG (M06)	ΔG (wB97XD)
$[Rh^{III}(C\text{-im-pyH}^+)(H_2O)_2I_2Cl]^+$	−54	−60
$[Rh^{I}(C\text{-im-pyH}^+)(OAc)(ethylene)]^+$	−22	−30
$[Rh^{I}(C\text{-im-pyH}^+)(COD)Cl]^+$ (**1a**)	−21	−23
$[Rh^{III}(C\text{-im-pyH}^+)(OAc)I_2(ethylene)]^+$	−21	−22
$[Rh^{I}(C\text{-im-pyH}^+)(H_2O)_2Cl]^+$	−7	−1.6
$[Me\text{-pyH}]^+$ ($\mathbf{9}^+$)	0	0
$[Rh^{III}(C,C'\text{-im-py})(H_2O)_2I_2]^+$ (**2**)	+24	+25
$[Rh^{III}(C,C'\text{-im-py})(OAc)I_2]^0$ (**3**)	+44	+41
$[Rh^{I}(C,C'\text{-im-py})(COD)]^+$	+45	+46
$[Rh^{I}(C,C'\text{-im-py})(H_2O)_2]^+$	+69	+73
$[Rh^{I}(C,C'\text{-im-py})(OAc)]^0$	+92	+96

[a]Geometries and included ZPVE correction calculated at M06-L/def2-SVP level; SMD solvent model.

CONCLUSIONS

Some lessons and predictions follow from this study.

(i) *o*-Metalation of the pyridinium ring of the *C*-im-pyH ligand in low-valent metal complexes such as $\mathbf{1}^+$ is a facile process. *o*-Metalation presumably occurs by an oxidative addition step and affords higher-valent metal complexes bound by the unusual asymmetric dicarbene chelate ligand, *C*,*C*′-im-py, such as the rhodium(II) dimers (**4-anti**, **4-syn**) and rhodium(III) monomers (**2**, **3**, **5**, **6**, and **7**) uncovered by this work.

(ii) DFT calculations for rhodium complexes **1**−**3** and some hypothetical analogues suggest that hydride transfer to the *C*,*C*′-im-py ligand is possible, but is energetically uphill compared to hydride transfer to the *C*-im-pyH$^+$ ligand.

(iii) The *C*,*C*′-im-py ligand is electrochemically silent over a wide potential range: processes that could be centered on this ligand were not observed between about −2.3 V (vs. the Fc$^+$/Fc couple) and the anodic solvent limit at about > +1.6 V (vs the Fc$^+$/Fc couple).

(iv) The DFT calculations reveal hydride addition to a pyridylidene NHC-ligand is energetically more favorable for higher oxidation state metal species. Such hydride addition reactions will most likely be found when the coligands that stabilize the pyridylidene-metal complex are difficult to reduce.

(v) A caveat to points (ii)−(iv) is that if reduction of the *C*,*C*′-im-py ligand to give the corresponding dihydro-*C*,*C*′-im-pyH ligand does occur, then the resulting metal species will be a powerful hydride donor.

(vi) The consistent difference in Rh−C_{NHC} bond lengths, indicative of weaker metal-binding of the pyridylidene carbene compared to the imidazolylidene carbene, is due to intramolecular steric interactions imposed by the different ring sizes in the rigid *C*,*C*′-im-pyH chelate ligand.

(vii) The (*C*′*C*-im-py)Rh complexes reported in this work are all rugged and easily handled: they are air and moisture stable, and soluble in a wide range of solvents. Diverse coordination chemistry is anticipated for these unusual dicarbene chelate ligands.

dx.doi.org/10.1021/ic202164v | *Inorg. Chem.* 2012, 51, 2191−2203

(viii) The *C′C*-im-py ligand may be useful as an inert, chelating coligand. That it is electrochemically silent over a wide potential range, particularly upon reduction, suggests utility in, for example, metallo-photosensitizers or phosphors to direct charge transfer from the metal to specific redox noninnocent ligands in the excited state.

In summary, facile metalation of the pyridinium cation presents problems for use of metal complexes of the *C*-im-pyH_2 ligand in hydride transfer reactions. We believe that this problem can be overcome by careful redesign of the hydride donor ligand and by forming metal complexes with multiple nicotinamide centers (so that oxidative addition does not inactivate all of them). Regardless, the new dicarbene *C,C′*-im-py offers considerable potential as an inert chelate ligand that forms robust, easily handled metal complexes.

EXPERIMENTAL SECTION

General Information. All organic reagents unless specified were purchased from commercial sources and used as received. Precursors 3-(*N,N*-di(*iso*-propyl)carboxamide)-1-methyl-5-(3-methyl-1*H*-imidazol-3-ium-1-yl)pyridinium diiodide ((Him-pyH)I_2),[8] [Rh(*C*-im-pyH)(COD)X][PF_6] (X = Cl, I)[8] and [Rh(COD)Cl]$_2$[26] were prepared by literature methods. Except where stated, the procedures were performed in air.

Preparations. **[Rh(*C,C′*-im-py)(H_2O)$_2$$I_2$][$PF_6$] (2).** (Him-pyH)$I_2$ (100 mg, 0.18 mmol) and [Rh(COD)Cl]$_2$ (44 mg, 0.09 mmol) were dissolved in acetonitrile (10 mL). Triethylamine (22 mg, 0.22 mmol) was added, at which point the solution immediately turned bright orange-red. The solution was stirred for 30 min, and the solvent purged from the reaction mixture using a stream of dinitrogen. The red residue was redissolved in the minimum amount of methanol, and added dropwise to a saturated aqueous solution of potassium hexafluorophosphate. To this was added acetone until the red precipitate was seen to fully dissolve. Slow evaporation in air gave the title compound as orange needles that were suitable for X-ray crystallography. Yield: 105 mg, 70%. (+)-ESI-MS *m/z* 697 ([M^+ − 2H_2O + MeCN]$^+$, 100%). ^{1}H NMR (500 MHz, CD_3CN): δ 8.35 (d, *J* = 1 Hz, 1H, py-**H**), 7.89 (d, *J* = 1 Hz, 1H, py-**H**), 7.88 (d, *J* = 2 Hz, 1H, im-**H**), 7.68 (d, *J* = 2 Hz, 1H, im-**H**), 4.53 (s, 3H, C**H**$_3$-N$_{py}$), 4.07 (s, 3H, C**H**$_3$-N$_{im}$), 3.72 (t, br, *J* = 6.4 Hz, 2H, (Me)$_2$C-**H**), 1.47 (s, br, 6H, C**H**$_3$-C), 1.20 (s, br, 6H, C**H**$_3$-C). ^{13}C{^{1}H} NMR (100.6 MHz, CD_3CN): δ 175.83 (d, J_{C-Rh} = 36.9 Hz, **C**$_{py}$), 163.49 (C═O), 162.03 (d, J_{C-Rh} = 40.9 Hz, **C**$_{im}$), 147.19, 139.69, 133.03, 127.02, (Ar-**C**), 54.10 ((Me)$_2$**C**-H), 38.13 (**C**H$_3$−N$_{py}$), 29.95 (**C**H$_3$−N$_{im}$), 19.80 (**C**H$_3$−C). The residual solvent peak conceals two im-py peaks. Anal. Calcd. for $C_{17}H_{28}F_6I_2N_4O_3PRh$: C, 25.36; H, 3.50; N, 6.96. Found: C, 25.25; H, 3.38; N 7.01%.

[Rh(*C,C′*-im-py)(OAc)I_2] (3), *anti/syn*-[Rh$_2$(*C,C′*-im-py)$_2$(OAc)$_2$$I_2$] (4-*anti*, 4-*syn*). Precursor (Him-pyH)I_2 (59 mg, 0.11 mmol), [Rh(COD)Cl]$_2$ (26 mg, 0.05 mmol), sodium acetate (72 mg, 0.88 mmol), and sodium iodide (79 mg, 0.53 mmol) in dry acetonitrile (10 mL) were heated at reflux under a nitrogen atmosphere for 5 h. The resulting orange-red solution was filtered and the solvent removed. The crude red residue was purified by column chromatography on silica gel (pore size 60 Å, 220−440 mesh) using dichloromethane-methanol (95:5) as eluent. [Rh(*C,C′*-im-py)(OAc)I_2] eluted first (orange), followed by *anti*-[Rh$_2$(*C,C′*-im-py)$_2$(OAc)$_2$$I_2$] (red), then *syn*-[Rh$_2$(*C,C′*-im-py)$_2(OAc)_2$$I_2$] (red).

Data for **3**: Crystallized from dichloromethane-hexane as orange crystals. Yield: 16.5 mg (20%). (+)-ESI-MS *m/z* 697 ([*M* − acetate + MeCN]$^+$, 100%). ^{1}H NMR (300 MHz, CD_3CN): δ 8.30 (d, *J* = 1 Hz, 1H, py-**H**), 7.84 (d, *J* = 2 Hz, 1H, im-**H**), 7.78 (d, *J* = 1 Hz, 1H, py-**H**), 7.39 (d, *J* = 2 Hz, 1H, im-**H**), 4.58 (s, 3H, C**H**$_3$-N$_{py}$), 4.06 (s, 3H, C**H**$_3$-N$_{im}$), 3.77 (s, br, 2H, (Me)$_2$C-**H**), 1.90 (s, 3H, C**H**$_3$CO$_2^-$) 1.39 (s, br, 12H, C**H**$_3$-C). ^{13}C{^{1}H} NMR (150.9 MHz, CD_3CN): δ 187.29 (**C**O$_2^-$), 183.65 (d, J_{C-Rh} = 34.6 Hz, **C**$_{py}$), 167.72 (d, J_{C-Rh} = 41.7 Hz, **C**$_{im}$), 164.39 (C═O), 147.83, 138.37, 132.15, 126.87, 117.27, 116.40 (Ar-**C**), 52.03 (br, (Me)$_2$**C**-H), 50.18 (**C**H$_3$CO$_2^-$), 46.50 (br, (Me)$_2$**C**-H), 35.72 (**C**H$_3$−N$_{py}$), 24.07 (**C**H$_3$−N$_{im}$), 20.18 (**C**H$_3$−C). UV−vis (MeCN): λ 264 (3.19×10^4 M^{-1} cm^{-1}), 331 (2.60×10^4 M^{-1} cm^{-1}), 419 (1.71×10^3 M^{-1} cm^{-1}). Anal. Calcd. for $C_{19}H_{27}I_2N_4O_3Rh$: C, 31.87; H, 3.80; N, 7.82. Found: C, 32.03; H, 3.85; N 7.79%.

Data for **4-*anti***: Crystallized from dichloromethane-hexane as red crystals. Yield: 22.5 mg (36%). (+)-ESI-MS *m/z* 1051 ([*M* − I]$^+$, 100%). ^{1}H NMR (300 MHz, CD_3CN): δ 7.56 (d, *J* = 1 Hz, 1H, py-**H**), 7.13 (d, *J* = 2 Hz, 1H, im-**H**), 6.97 (d, *J* = 1 Hz, 1H, py-**H**), 6.75 (d, *J* = 2 Hz, 1H, im-**H**), 4.08 (s, 3H, C**H**$_3$-N$_{py}$), 3.70 (s, 3H, C**H**$_3$-N$_{im}$), 3.65 (s, br, 2H, (Me)$_2$C-**H**), 1.27 (s, br, 12H, C**H**$_3$-C). ^{13}C{^{1}H} NMR (125.8 MHz, CD_3CN): δ 195.24 (d, J_{C-Rh} = 57.9 Hz, **C**$_{py}$), 183.46 (**C**O$_2^-$), 177.68 (d, J_{C-Rh} = 52.6 Hz, **C**$_{im}$), 165.24 (C═O), 146.11, 137.13, 127.27, 124.67, 115.45, 112.40 (Ar-**C**), 51.08 (br, (Me)$_2$**C**-H), 50.39 (**C**H$_3$CO$_2^-$), 46.50 (br, (Me)$_2$**C**-H), 36.05 (**C**H$_3$−N), 23.73 (**C**H$_3$−N), 19.84 (**C**H$_3$−C). The residual solvent peak conceals one im-py peak. UV−vis (MeCN): λ 240 (3.60×10^4 M^{-1} cm^{-1}), 288 (1.21×10^4 M^{-1} cm^{-1}), 375 (1.68×10^4 M^{-1} cm^{-1}). Anal. Calcd. for $C_{38}H_{54}I_2N_8O_6Rh_2 \cdot 2H_2O$: C, 37.58; H, 4.81; N, 9.23. Found: C, 37.39; H, 4.81; N 8.97%.

Data for **4-*syn***: Crystallized from dichloromethane-hexane as red crystals. Yield: 11.4 mg, (9%). (+)-ESI-MS *m/z* 1051 ([*M* − I]$^+$, 100%). ^{1}H NMR (300 MHz, CD_3CN): δ 7.54 (d, *J* = 1 Hz, 1H, py-**H**), 7.15 (d, *J* = 2 Hz, 1H, im-**H**), 6.94 (d, *J* = 1.3 Hz, 1H, py-**H**), 6.81 (d, *J* = 2 Hz, 1H, im- **H**), 4.03 (s, 3H, C**H**$_3$-N$_{py}$), 3.65 (s, 3H, C**H**$_3$-N$_{im}$), 3.60 (s, br, 2H, (Me)$_2$C-**H**), 1.25 (s, br, 12H, C**H**$_3$-C).

*[Rh(C,C′-im-py)(PhCO$_2$)I_2] (**5**).* Procedure as for [**Rh(*C,C′*-im-py)(OAc)I_2**], but using sodium benzoate. [**Rh(*C,C′*-im-py)(PhCO$_2$)-I_2**] (**5**) eluted first (orange). A mixture of products eluted next (red) which contained [**Rh$_2$(*C,C′*-im-py)$_2$(PhCO$_2$)$_2$$I_2$**] (by (+)-ESI-MS, *m/z* 1175 ([*M* − I]$^+$) and a number of other unidentified products. Product **5** was crystallized from acetonitrile at −15 °C as orange needles. Yield from 50 mg (0.09 mmol) (Him-pyH)I_2: 13.3 mg, (19%). ESI-MS *m/z* 697 ([*M* − PhCO$_2$ + MeCN]$^+$, 100%). ^{1}H NMR (500 MHz, CD_3CN): δ 8.34 (s, 1H, im-py), 8.07 (d, *J* = 8 Hz, 2H, *o*-Ph-**H**), 7.87 (d, *J* = 2 Hz, 1H, im-py), 7.82 (s, 1H, im-py), 7.61 (t, *J* = 8 Hz, 1H, *p*-Ph-**H**), 7.52 (t, *J* = 8 Hz, 2H, *m*-Ph-**H**), 7.42 (d, *J* = 2 Hz, 1H, im-py), 4.71 (s, 3H, C**H**$_3$-N), 4.19 (s, 3H, C**H**$_3$-N), 3.78 (s, br, 2H, (Me)$_2$C-**H**), 1.35 (s, br, 12H, C**H**$_3$-C). Anal. Calcd. for $C_{24}H_{29}I_2N_4O_3Rh$: C, 37.04; H, 3.76; N, 7.20. Found: C, 37.10; H, 3.71; N 7.00%.

*[Rh(C,C′-im-py)(ArCO$_2$)I_2], Ar = CPh$_3$ (**6**), C$_2$Ph$_6$ (**7**).* Freshly cut sodium (5 g, 217 mmol) was added to trityl chloride (3.61 g, 12.9 mmol) in dry diethyl ether (100 mL) under a nitrogen atmosphere. The reaction mixture was stirred vigorously overnight to give a bright red solution. Dry carbon dioxide was bubbled through this solution. An immediate color change from red to pale yellow-green was observed. The mixture was stirred for 30 min under a carbon dioxide atmosphere, and then filtered, and the solid residue washed with copious ethyl acetate. The solvent was removed from the combined liquors to afford yellow oil. This was passed through a short column (5 cm) of silica (pore size 60 Å, 220−440 mesh) using ethyl acetate as eluent. The second yellow band was collected, and the solvent removed to afford a cream powder (354 mg). (Him-pyH)I_2 (50 mg, 0.09 mmol), [Rh(COD)Cl]$_2$ (44 mg, 0.09 mmol), the aforementioned powder (150 mg, ∼0.5 mmol) and sodium iodide (79 mg, 0.68 mmol) in dry acetonitrile (10 mL) were heated at reflux under a nitrogen atmosphere for 7 days. The resulting orange suspension was filtered and subjected to chromatography as for **3**, **4-*anti***, and **4-*syn***. Complex **6** eluted first (orange band), followed by **7** (orange band).

Data for **6**: Crystallized from dichloromethane-ethanol as orange crystals. Yield from 50 mg (0.09 mmol) (Him-pyH)I_2: 24 mg, (30%). (+)-ESI-MS *m/z* 697 ([*M* − carboxylate + MeCN]$^+$, 100%). ^{1}H NMR (500 MHz, ((CD$_3$)$_2$CO): δ 8.65 (s, 1H, im-py), 8.23 (d, *J* = 2 Hz, 1H, im-py), 8.10 (s,1H, im-py), 7.62 (d, *J* = 2 Hz, 1H, im-py), 7.45 (dd, *J* = 2, 8 Hz, 6H, *o*-Ph-**H**)), 7.24−7.28 (m, 9H, *m/p*-Ph-**H**), 4.64 (s, 3H, C**H**$_3$-N), 4.06 (s, 3H, C**H**$_3$-N), 3.87 (s, br, 2H, (Me)$_2$C-**H**), 1.39 (s, br, 12H, C**H**$_3$-C). Anal. Calcd. for $C_{37}H_{39}I_2N_4O_3Rh$: C, 47.05; H, 4.16; N, 5.93. Found: C, 46.60; H, 3.93; N 5.70%.

dx.doi.org/10.1021/ic202164v | *Inorg. Chem.* 2012, 51, 2191−2203

Data for **7**: Crystallized from hot dichloromethane-acetonitrile as orange crystals. Yield from 50 mg (0.09 mmol) (Him-pyH)I_2: 5 mg, (5%). (+)-ESI-MS *m/z* 697 ([*M* − carboxylate + MeCN]$^+$, 100%). ^{1}H NMR (600 MHz, ($(CD_3)_2SO$): δ 8.72 (s, 1H, im-py), 8.37 (s,1H, im-py), 8.27 (s,1H, im-py), 7.69 (s, 1H, im-py), 7.00−7.32 (m, 29H, Ph-**H**)), 4.48 (s, 3H, C**H**$_3$-N), 3.93 (s, 3H, C**H**$_3$-N), 3.70 (s, br, 2H, $(Me)_2$C-**H**), 1.46 (s, br, 6H, C**H**$_3$-C), 1.21 (s, br, 6H, C**H**$_3$-C). Anal. Calcd. for $C_{56}H_{53}I_2N_4O_3Rh$: C, 56.68; H, 4.50; N, 4.72. Found: C, 56.22; H, 4.71; N 5.02%.

Physical Measurements. ^{1}H and $^{13}C\{^1H\}$ spectra were recorded on Bruker Avance 300, 500, and 600 MHz spectrometers at 298 K. Positive ion-mode ESI-mass spectra were recorded on a Finnigan LCQ DecaXP Quadrupole Ion Trap Mass Spectrometer. Elemental analyses were performed by the Microanalytical Unit of the Research School of Chemistry, Australian National University. Samples for elemental analysis were dried at 30 °C over phosphorus pentoxide in vacuo for at least 7 days.

Electrochemical Measurements. Cyclic voltammetry was performed as described in detail elsewhere[27] with a Pine Instrument Co. AFCBP1 bipotentiostat. A three-electrode system was used, consisting of a glassy carbon working electrode, a platinum counter electrode, and a Ag/AgCl reference electrode. UV−visible spectroelectrochemical experiments were carried out on a Cary 50 Bio diode-array spectrometer with an airtight UV−vis-NIR cuvette (1 mm path-length) with a light-transparent platinum gauze working electrode. High-purity N_2 was used to deoxygenate the solution before each electrochemical and spectroelectrochemical experiment.

X-ray Crystallography. Single Crystal X-ray Diffraction data collection was carried out at 150 K on a Bruker Kappa diffractometer using graphite-monochromated Mo Kα radiation (λ = 0.71073 Å) and an APEX-II CCD detector. The structures were solved by direct and Fourier methods and refined by full-matrix least-squares on F^2 using SHELX-97[28] software packages.

DFT Calculations. DFT calculations were performed primarily using the Gaussian 09 software package[29] using restricted closed-shell wave functions. Geometry optimizations and frequency calculations were carried out in vacuum at the M06-L/def2-SVP level of theory.[30] Single point energy calculations employed the larger def2-TZVP basis set. Three functionals were employed, specifically M06-L,[30a] M06,[30a] and wB97X-D,[31] and energies were calculated both in vacuum and in acetonitrile solvent. Where calculations in solvent are indicated, the SMD method of Truhlar et al. with acetonitrile as solvent was employed as implemented in Gaussian09.[32] Energies quoted include correction for zero-point vibrational energy calculated using M06-L/def2-SVP. A scaling factor of 0.98 was used for scaling of the zero-point vibrational energy value.[33] Further details are given in the Supporting Information. NMR parameters were calculated using the ADF software package[34] (see footnote of Table 4 for details).

■ ASSOCIATED CONTENT

Supporting Information

Crystal structure data for complexes **2**, **3**, **4-*anti***, **4-*syn***, and **7** (CIF files), additional electrochemical results, full experimental details for the DFT calculations, the full citation for ref 29, and estimated energies and atomic coordinates from DFT calculations. This material is available free of charge via the Internet at http://pubs.acs.org.

■ AUTHOR INFORMATION

Corresponding Author

*E-mail: s.colbran@unsw.edu.au.

■ REFERENCES

(1) (a) You, S. L. *Chem.—Asian J.* **2007**, *2*, 820−827. (b) Ouellet, S. G.; Walji, A. M.; Macmillan, D. W. C. *Acc. Chem. Res.* **2007**, *40*, 1327−1339. (c) Connon, S. J. *Org. Biomol. Chem.* **2007**, *5*, 3407−3417. (d) Rueping, M.; Dufour, J.; Schoepke, F. R. *Green Chem.* **2011**, *13*, 1084−1105. (e) Kanomata, N.; Nakata, T. *Angew. Chem., Int. Ed. Engl.* **1997**, *36*, 1207−1211. (f) Burgess, V. A.; Davies, S. G.; Skerlj, R. T.; Whittaker, M. *Tetrahedron: Asymmetry* **1992**, *3*, 871−901. (g) Burgess, V. A.; Davies, S. G.; Skerlj, R. T. *Tetrahedron: Asymmetry* **1991**, *2*, 299−328. (h) Martin, N. J. A.; List, B. *J. Am. Chem. Soc.* **2006**, *128*, 13368−13369. (i) Li, G. L.; Liang, Y. X.; Antilla, J. C. *J. Am. Chem. Soc.* **2007**, *129*, 5830−5831. (j) Jouin, P.; Troostwijk, C. B.; Kellogg, R. M. *J. Am. Chem. Soc.* **1981**, *103*, 2091−2093. (k) Reichenbach-Klinke, R.; Kruppa, M.; Konig, B. *J. Am. Chem. Soc.* **2002**, *124*, 12999−13007. (l) Fukuzumi, S.; Nishizawa, N.; Tanaka, T. *J. Chem. Soc., Perkin Trans. 2* **1985**, 371−378. (m) Fukuzumi, S.; Yuasa, J.; Yamada, S. *J. Am. Chem. Soc.* **2006**, *128*, 14938−14948.

(2) Fukuzumi, S.; Koumitsu, S.; Hironaka, K.; Tanaka, T. *J. Am. Chem. Soc.* **1987**, *109*, 305−316.

(3) (a) Moracci, F. M.; Liberatore, F.; Carelli, V.; Arnone, A.; Carelli, I.; Cardinali, M. E. *J. Org. Chem.* **1978**, *43*, 3420−3422. (b) Carelli, V.; Liberatore, F.; Casini, A.; Tortorella, S.; Scipione, L.; Di Rienzo, B. *New J. Chem.* **1998**, *22*, 999−1004. (c) Anne, A.; Hapiot, P.; Moiroux, J.; Saveant, J. M. *J. Electroanal. Chem.* **1992**, *331*, 959−970.

(4) (a) Acheson, R. M.; Paglietti, G. *J. Chem. Soc., Perkin Trans. 1* **1976**, 45−48. (b) Eisner, U.; Kuthan, J. *Chem. Rev.* **1972**, *72*, 1−42.

(5) (a) Westerhausen, D.; Herrmann, S.; Hummel, W.; Steckhan, E. *Angew. Chem., Int. Ed. Engl.* **1992**, *31*, 1529−1531. (b) Lo, H. C.; Leiva, C.; Buriez, O.; Kerr, J. B.; Olmstead, M. M.; Fish, R. H. *Inorg. Chem.* **2001**, *40*, 6705−6716. (c) Holmann, F.; Kleeb, A.; Otto, K.; Schmid, A. *Tetrahedron: Asymmetry* **2005**, *16*, 3512−3519. (d) Hollmann, F.; Witholt, B.; Schmid, A. *J. Mol. Catal. B: Enzym.* **2002**, *19*, 167−176. (e) Hollmann, F.; Grau, M. M.; Poizat, M.; Arends, I. W. C. E. *Appl. Organomet. Chem.* **2010**, *24*, 380−385. (f) Wagenknecht, P. S.; Penney, J. M.; Hembre, R. T. *Organometallics* **2003**, *22*, 1180−1182. (g) Steckhan, E.; Herrmann, S.; Ruppert, R.; Dietz, E.; Frede, M.; Spika, E. *Organometallics* **1991**, *10*, 1568−1577. (h) Ruppert, R.; Herrmann, S.; Steckhan, E. *J. Chem. Soc., Chem. Commun.* **1988**, 1150−1151. (i) Fish, R. H.; Lo, H. C.; Leiva, C.; Buriez, O.; Kerr, J. B.; Olmstead, M. M. *Inorg. Chem.* **2001**, *40*, 6705−6716. (j) Fish, R. H.; Lo, H. C.; Buriez, O.; Kerr, J. B. *Angew. Chem., Int. Ed.* **1999**, *38*, 1429−1432.

(6) Chen, Q.-A.; Chen, M.-W.; Yu, C.-B.; Shi, L.; Wang, D.-S.; Yang, Y.; Zhou, Y.-G. *J. Am. Chem. Soc.* **2011**, *133* (41), 16432−16435.

(7) (a) Zhu, X. Q.; Zhang, M. T.; Yu, A.; Wang, C. H.; Cheng, J. P. *J. Am. Chem. Soc.* **2008**, *130*, 2501−2516. (b) Richter, D.; Tan, Y.; Antipova, A.; Zhu, X.-Q.; Mayr, H. *Chem.—Asian J.* **2009**, *4*, 1824−1829.

(8) McSkimming, A.; Bhadbhade, M.; Colbran, S. B. *Dalton Trans.* **2010**, *39*, 10581−10584.

(9) (a) Wolf, S.; Plenio, H. *J. Organomet. Chem.* **2009**, *694*, 1487−1492. (b) Chianese, A. R.; Li, X. W.; Janzen, M. C.; Faller, J. W.; Crabtree, R. H. *Organometallics* **2003**, *22*, 1663−1667. (c) Frey, G. D.; Rentzsch, C. F.; von Preysing, D.; Scherg, T.; Muhlhofer, M.; Herdtweck, E.; Herrmann, W. A. *J. Organomet. Chem.* **2006**, *691*, 5725−5738. (d) Crudden, C. M.; Praetorius, J. M. *Dalton Trans.* **2008**, 4079−4094.

(10) Albrecht, M.; Crabtree, R. H.; Mata, J.; Peris, E. *Chem. Commun.* **2002**, 32−33.

(11) (a) Tomboulian, P. *J. Org. Chem.* **1959**, *24*, 229−234. (b) Lankamp, H.; Nauta, W. T.; Maclean, C. *Tetrahedron Lett.* **1968**, 249−254.

(12) (a) Arnold, P. L.; Pearson, S. *Coord. Chem. Rev.* **2007**, *251*, 596−609. (b) Schuster, O.; Yang, L. R.; Raubenheimer, H. G.; Albrecht, M. *Chem. Rev.* **2009**, *109*, 3445−3478. (c) Frenking, G.; Nemcsok, D.; Wichmann, K. *Organometallics* **2004**, *23*, 3640−3646. (d) Schuster, O.; Stander-Grobler, E.; Heydenrych, G.; Cronje, S.; Tosh, E.; Albrecht, M.; Frenking, G.; Raubenheimer, H. G. *Organometallics* **2010**, *29*, 5821−5833. (e) Raubenheimer, H. G.; Cronje, S. *Dalton Trans.* **2008**, 1265−1272.

(13) Quezada, C. A.; Garrison, J. C.; Panzner, M. J.; Tessier, C. A.; Youngs, W. J. *Organometallics* **2004**, *23*, 4846−4848.

(14) Conejero, S.; Rosello-Merino, M.; Diez, J. *Chem. Commun.* **2010**, *46*, 9247−9249.

(15) (a) Crawford, C. A.; Matonic, J. H.; Huffman, J. C.; Folting, K.; Dunbar, K. R.; Christou, G. *Inorg. Chem.* **1997**, *36*, 2361−2371. (b) Calligaris, M.; Campana, L.; Mestroni, G.; Tornatore, M.; Alessio, E. *Inorg. Chim. Acta* **1987**, *127*, 103−112. (c) Yoshimura, T.; Umakoshi, K.; Sasaki, Y. *Inorg. Chem.* **2003**, *42*, 7106−7115. (d) Cotton, F. A.; Dunbar, K. R.; Verbruggen, M. G. *J. Am. Chem. Soc.* **1987**, *109*, 5498−5506.
(16) (a) Fujihara, T.; Obora, Y.; Tokunaga, M.; Tsuji, Y. *Dalton Trans.* **2007**, 1567−1569. (b) Poyatos, M.; Sanau, M.; Peris, E. *Inorg. Chem.* **2003**, *42*, 2572−2576. (c) Song, H. B.; Gu, L. N.; Zi, G. F. *J. Organomet. Chem.* **2009**, *694*, 1493−1502.
(17) (a) Cotton, F. A.; Murillo, C. A.; Stiriba, S. E. *Inorg. Chem. Commun.* **1999**, *2*, 463−464. (b) Fernandez, R.; Magriz, A.; Gomez-Bujedo, S.; Alvarez, E.; Lassaletta, J. M. *Organometallics* **2010**, *29*, 5941−5945. (c) Fernandez, R.; Gomez-Bujedo, S.; Alcarazo, M.; Pichon, C.; Alvarez, E.; Lassaletta, J. M. *Chem. Commun.* **2007**, 1180−1182.
(18) For citations to the electrochemistry of iodide ion in various media, see: Rogers, E. I.; Streeter, I.; Aldous, L.; Hardacre, C.; Compton, R. G. *J. Phys. Chem. C* **2008**, *112*, 10976−10981.
(19) The concurrence of the UV−vis bands of **3** with those anticipated for a dihydropyridine derivative is coincidental: the NMR and UV−vis spectra for the same sample of **3** were checked and are as reported.
(20) (a) Lopez-Alarcon, C.; Squella, J. A.; Miranda-Wilson, D.; Nunez-Vergara, L. J. *Electroanalysis* **2004**, *16*, 539−546. (b) Leduc, P.; Thevenot, D. *J. Electroanal. Chem.* **1973**, *47*, 543−546. (c) Blaedel, W. J.; Haas, R. G. *Anal. Chem.* **1970**, *42*, 918−927.
(21) (a) Pruchnik, F. P.; Rak, M.; Gunik, L. Z.; Lafolet, F.; Chardon-Noblat, S.; Deronzier, A. *Eur. J. Inorg. Chem.* **2009**, 111−118. (b) Lafolet, F.; Chardon-Noblat, S.; Duboc, C.; Deronzier, A.; Pruchnik, F. P.; Rak, M. *Dalton. Trans.* **2008**, 2149−2156. (c) Pruchnik, F. P.; Jutarska, A.; Ciunik, Z.; Pruchnik, M. *Inorg. Chim. Acta* **2003**, *350*, 609−616. (d) Pruchnik, F. P.; Jakimowicz, P.; Ciunik, Z.; Stanislawek, K.; Oro, L. A.; Tejel, C.; Ciriano, M. A. *Inorg. Chem. Commun.* **2001**, *4*, 19−22. (e) Pruchnik, F. P.; Cwikowska, M.; Pavlyuk, O.; Lafolet, F.; Chardon-Noblat, S.; Deronzier, A. *Polyhedron* **2010**, *29*, 3059−3065.
(22) Crawford, C. A.; Matonic, J. H.; Streib, W. E.; Huffman, J. C.; Dunbar, K. R.; Christou, G. *Inorg. Chem.* **1993**, *32*, 3125−3133.
(23) (a) Cabeza, J. A.; del Rio, I.; Goite, M. C.; Perez-Carreno, E.; Pruneda, V. *Chem.—Eur. J.* **2009**, *15*, 7339−7349. (b) Cabeza, J. A.; del Rio, I.; Perez-Carreno, E.; Pruneda, V. *Chem.—Eur. J.* **2010**, *16*, 5425−5436. (c) Cabeza, J. A.; del Rio, I.; Perez-Carreno, E.; Pruneda, V. *Organometallics* **2011**, *30*, 1148−1156.
(24) Tanaka, K.; Padhi, S. K.; Kobayashi, K.; Masuno, S. *Inorg. Chem.* **2011**, *50*, 5321−5323.
(25) (a) Ziegler, T.; Krykunov, M.; van Lenthe, E. *J. Phys. Chem. A* **2009**, *113*, 11495−11500. (b) Autschbach, J.; Moncho, S. *J. Chem. Theory Comput.* **2010**, *6*, 223−234.
(26) Giordano, G.; Crabtree, R. H. *Inorg. Synth.* **1990**, *28*, 88−90.
(27) (a) Evans, A. J.; Watkins, S. E.; Craig, D. C.; Colbran, S. B. *Dalton Trans.* **2002**, 983−994. (b) Colbran, S. B.; Lee, S. T.; Lonnon, D. G.; Maharaj, F. J. D.; McDonagh, A. M.; Walker, K. A.; Young, R. D. *Organometallics* **2006**, *25*, 2216−2224. (c) Lonnon, D. G.; Lee, S. T.; Colbran, S. B. *J. Am. Chem. Soc.* **2007**, *129*, 5800−5801.
(28) Sheldrick, G. M. *SHELX-97*; University of Göttingen: Göttingen, Germany, 1997.
(29) Frisch, M. J. et al. *Gaussian 09*, Revision A.1; Gaussian, Inc.: Wallingford, CT, 2009.
(30) (a) Weigend, F.; Ahlrichs, R. *Phys. Chem. Chem. Phys.* **2005**, *7*, 3297−3305. (b) Truhlar, D. G.; Zhao, Y. *Acc. Chem. Res.* **2008**, *41*, 157−167.
(31) Head-Gordon, M.; Chai, J. D. *Phys. Chem. Chem. Phys.* **2008**, *10*, 6615−6620.
(32) Cramer, C. J.; Marenich, A. V.; Truhlar, D. G. *J. Phys. Chem. B* **2009**, *113*, 6378−6396.
(33) "Database of Frequency Scaling Factors for Electronic Structure Methods" (maintained by Zheng, J.; Lynch, B. J.; Zhao, Y.; Truhlar, D. G.;) http://comp.chem.umn.edu/freqscale/version3b1.htm
(34) *ADF software package*, v2010.02; Scientific Computing & Modelling: Amsterdam, The Netherlands, 2010.